2022 American Control Conference (ACC)
Atlanta, USA, June 8-10, 2022

Shape Estimation of Soft Manipulators using Piecewise Continuous Pythagorean-Hodograph Curves

Harish Bezawada, Cole Woods and Vishesh Vikas[1]

***Abstract*—In recent years, there has been significant interest in use of soft and continuum manipulators in diverse fields including surgical and agricultural robotics. Consequently, researchers have designed open-loop and feedback control algorithms for such systems. Here, the knowledge of the manipulator shape is critical for effective control. The estimation of the manipulator shape is challenging due to their highly deformable and non-linear nature. Researchers have explored inductive, magnetic and optical sensing techniques to deduce the manipulator shape. However, they are intrusive and economically expensive. Alternate non-contact sensing approaches may involve use of vision or inertial measurement units (IMUs) that are placed at known intervals along the manipulator. Here, the camera provides position of the marker, while the slope (rotation matrix or direction cosines) can be determined using IMUs. In this paper, we mathematically model the manipulator shape using multiple piecewise continuous quintic Pythogorean-Hodograph (PH) curves. A PH-curve has continuous slope and is a convenient parametric model for curves with constant length. We investigate the use of multiple piecewise continuous-curvature PH curves to estimate the shape of a soft continuum manipulator. The curves model manipulator segments of constant lengths while the slopes at the knots are assumed to be known. For N curve segments with $(4N + 8)$ unknowns, the shape estimation is formulated as a constrained optimization problem that minimizes the curve bending energy. The algorithm imposes $(4N + 3)$ nonlinear constraints corresponding to continuity, slope and segment length. Unlike traditional cubic splines, the optimization problem is nonlinear and sensitive to initial guesses and has potential to provide incorrect estimates. We investigate the robustness of the algorithm by adding variation to the direction cosines, and compare the output shapes. The simulation results on a five-segment manipulator illustrate the robustness of the algorithm. While the experimental results on a soft tensegrity-spine manipulator validate the effectiveness of the approach. Here estimation error of the end-effector position normalized to the manipulator length are 6.53% and 6.2% for the two experimental poses.**

I. Introduction

In the recent years, soft material and continuum manipulators have gained prominence given their compliant and adaptable nature, and safety of operation near humans. Consequently, they have found diverse applications in fields of medical, wearable and agricultural robotics [1]–[5]. The control of such systems is approached using multiple techniques including model-based continuum curvature and cosserat-rod [6], [7]. Tensegrity spine-inspired manipulators display soft behavior of high deformability and flexibility with variable stiffness [8]. However, their modeling and control has proven to be challenging due to their nonlinear kinematic and dynamic nature [9].

The closed loop control of such systems requires reconstruction of the manipulator shape profile. Researchers have explored multiple active sensors that employ resistive, inductive, magnetic and optical principles. Resistive sensors using conducting composites are influenced by environmental factors like temperature and humidity [10], [11]. Stretchable sensors have been used for shape estimation of a surgical robot [12]. Although the sensors are easy to manufacture, care needs to be taken while attaching them to the electrodes, hence, also making it difficult to replace. Similarly, Fiber Bragg Grating sensors detecting reflected light need to be carefully embedded inside the robot body and affect the manipulator dynamics [13]–[17]. In short, these approaches have the drawback of being intrusive and economically expensive. Consequently, recent research has involved shape reconstruction using non-contact vision-feedback [18].

Another perspective for reconstructing shape profile is the use of curve interpolation techniques where the position or slope at given intervals of the manipulator are known, and the continuity of position, slope and curvature is maintained between these intervals. The use of cubic splines is prevalent for interpolating surfaces where the parametric curve between two points (referred to as 'knots') is a third degree polynomial. This approach offers the advantage of being linear and computationally cheap. However, when being applied to soft manipulators, the algorithm needs to incorporate an additional non-linear constraint corresponding to constant lengths between consecutive knots. The lack of an analytical solution to impose the length constraints makes the approach computationally expensive. In this context, a Printed Circuit Board ribbon with continuous arrangement of embedded sensors has been investigated [19]. In contrast, Pythagorean Hodograph (PH) curves have a special property of having constant slope which has analytical advantages when imposing length constraints [20], [21]. The use of PH curves with quaternions on a Robotonix XT rigid manipulator

*This work is supported by the National Science Foundation under Grant No. 1830432 and 1832993

[1]Harish Bezawada, Cole Woods and Vishesh Vikas are with the Agile Robotics Lab (ARL), University of Alabama, Tuscaloosa AL 36487, USA hbezawada@crimson.ua.edu, cswoods@crimson.ua.edu, vvikas@ua.edu

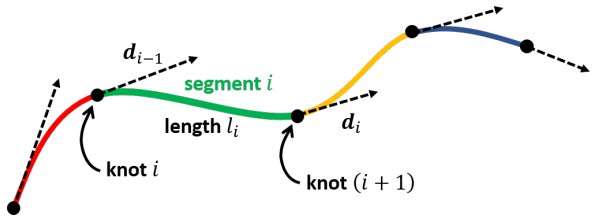

Fig. 1. Piecewise continuous modeling of a soft manipulator where the segment lengths l_i and the direction cosines (slopes) $\boldsymbol{d}_i$ are known at the knots.

has been explored where the whole manipulator is assumed as a single segment [22].

Contributions. The research mathematically models a soft tensegrity manipulator, Fig. 1, as piecewise PH curves of quinitic order. The sensors are located at constant lengths along the manipulator and the slope at each knot is assumed to be known. Mathematically, the curves are C^0, C^1, C^2 continuous at the knots. The paper uses multiple segments for a planar shape estimation problem using input of direction cosines at knots and the length between consecutive knots. The shape estimation with N segments, equivalently, $(4N+8)$ unknowns, is formulated as a nonlinear optimization problem that minimizes the curves' bending energy with $(4N+3)$ non-linear constraints. This is experimentally verified on a soft tensegrity-spine manipulator where the slopes are obtained using visual markers placed at known intervals along the manipulator. The robustness of the algorithm to the error in the slope (sensor noise) is investigated.

The remainder of the paper is organized as follows: Sec. II introduces the PH Curves and discusses the estimation algorithm along with the proof. Sec. III presents numerical simulation setup, tensegrity based spine model and robustness study of the estimation algorithm. It also discusses the simulation and the experimental results.

II. Parametric Model of Continuum Manipulator using PH-Curves

A. Pythagorean Hodograph (PH) Curves

PH-curves are beneficial to obtain closed form solutions when working with lengths of curves. The curve terminology and properties are summarized as

1) *Parametric representation* of the curve is $\boldsymbol{r}(h)$ with the normalized curvilinear coordinate $h \in [0,1]$

$$\boldsymbol{r}(h) = [x(h), y(h), z(h)]^T \tag{1}$$

where, x, y, z are spatial coordinates. However, the length of the curve L does not have a generic closed-form solution

$$L = \int_0^1 |\boldsymbol{r}'(h)|dh = \int_0^1 \sqrt{x'(h)^2 + y'(h)^2 + z'(h)^2}dh$$

2) *Hodograph* is the first derivative of the curve that satisfies the Pythogorean condition

$$\begin{aligned} &\boldsymbol{r}'(h) = [x'(h), y'(h), z'(h)]^T \\ \text{s.t.} \quad &x'(h)^2 + y'(h)^2 + z'(h)^2 = \sigma(h)^2 \end{aligned} \tag{2}$$

where $\sigma(h)$ is some function of h. The Pythogorean constraints facilitates closed form solution for the curve length.

$$L = \int_0^1 |\boldsymbol{r}'(h)|dh = \int_0^1 |\sigma(h)|dh \tag{3}$$

3) *Parametric hodographs* that allow for satisfaction of the Pythogorean condition are

$$\begin{aligned} x'(h) &= \left[u^2(h) + v^2(h) - p^2(h) - q^2(h)\right] \\ y'(h) &= 2\left[u(h)q(h) + v(h)p(h)\right] \\ z'(h) &= 2\left[v(h)q(h) - u(h)p(h)\right] \\ |\boldsymbol{r}'(h)| &= |\sigma(h)| = u^2(h) + v^2(h) + p^2(h) + q^2(h) \end{aligned} \tag{4}$$

where $u(h), v(h), p(h), q(h)$ are polynomials of any degree. Linear polynomials do not have any degree of freedom and are not feasible. Hence, quadratic polynomials with two degrees of freedom are considered which result in a *quintic PH-Curve*.

4) *The quadratic polynomials* can be written in Bernstein form

$$\begin{aligned} u(h) &= u_0(1-h)^2 + u_1 2(1-h)h + u_2 h^2 \\ v(h) &= v_0(1-h)^2 + v_1 2(1-h)h + v_2 h^2 \\ p(h) &= p_0(1-h)^2 + p_1 2(1-h)h + p_2 h^2 \\ q(h) &= q_0(1-h)^2 + q_1 2(1-h)h + q_2 h^2 \end{aligned}$$

and the Biezier form with five control points, $\boldsymbol{P}_k$

$$\boldsymbol{r}(h) = \sum_{k=0}^{5} \boldsymbol{P}_k \binom{5}{k} (1-h)^{5-k} h^k$$

We will use the Hopf representation of the PH-curves using third degree complex polynomials $\alpha(h), \beta(h)$

$$\begin{aligned} &\alpha(h) = u(h) + iv(h), \beta(h) = q(h) + ip(h) \\ &\text{s.t.} \quad x'(h) = |\alpha(h)|^2 - |\beta(h)|^2 \\ &y'(h) = 2Re(\alpha(h)\bar{\beta}(h)), z'(h) = 2Im(\alpha(h)\bar{\beta}(h)) \\ &\sigma(h)^2 = |\alpha(h)|^2 + |\beta(h)|^2 \end{aligned} \tag{5}$$

$\bar{\gamma}$ represent the complex conjugate of γ.

B. Manipulator shape estimation

Problem Definition. A soft manipulator has N sensors located at known intervals that give information about the slopes or direction cosines $\boldsymbol{d}_i$ and the segment length l_i as illustrated in Fig. 1(b). The shape is defined using segments of PH-curves $\boldsymbol{r}_i(h)$. It is desired to find the parametric representation of these curve segments that preserve positional C^0, tangential C^1 and curvature C^2 continuity, and are of constant length l_i.

Parametric representation ensuring continuity. Let the Hopf form quadratic polynomials for a segment i,

$(\alpha_i(h), \beta_i(h))$, be defined using complex coefficients $a_i, b_i, i = 0, \cdots, (N+1)$

$$\begin{aligned}\alpha_i(h) &= \frac{(a_{i-1}+a_i)}{2}(1-h)^2 + 2a_i(1-h)h + \frac{(a_i+a_{i+1})}{2}h^2 \\ \beta_i(h) &= \frac{(b_{i-1}+b_i)}{2}(1-h)^2 + 2b_i(1-h)h + \frac{(b_i+b_{i+1})}{2}h^2\end{aligned} \tag{6}$$

It can be easily observed that this presentation preserves C^1, C^2 continuity at the knots $i = 1, \cdots, N$.

$$\boldsymbol{r}_i'(1) = \boldsymbol{r}_{i+1}'(0), \quad \boldsymbol{r}_i''(1) = \boldsymbol{r}_{i+1}''(0)$$

Hence, for the shape defined using segments of PH-curves $\boldsymbol{r}_i(h)$ using the proposed parameterization, it is desired to calculate $4(N+2) = (4N+8)$ unknowns corresponding to the complex $a_i, b_i, i = 0, \cdots, (N+1)$.

Slope and length constraints. Let the slope or direction cosines at each knot be $\boldsymbol{d}_i = (dx_i, dy_i, dz_i)$. The relationship between the unknowns is

$$\begin{aligned}\boldsymbol{g}_i(a,b) &= \begin{bmatrix} \frac{1}{4}(|a_i + a_{i+1}|^2 - |b_i + b_{i+1}|^2) \\ Re\left(\frac{1}{2}(a_i + a_{i+1})(\bar{b}_i + \bar{b}_{i+1})\right) \\ Im\left(\frac{1}{2}(a_i + a_{i+1})(\bar{b}_i + \bar{b}_{i+1})\right) \end{bmatrix} = \boldsymbol{r}_i'(1) \\ \boldsymbol{g}_i - \boldsymbol{d}_i &= 0, \quad \forall i = 1, \cdots, (N+1)\end{aligned} \tag{7}$$

Hence, the slope readings at the knots provides $3(N+1)$ nonlinear equations. Similarly, let the length of a segment i be l_i, then analytically

$$\begin{aligned}L_i(a,b) = \int_0^1 |\boldsymbol{r}_i'(h)|dh = \frac{1}{120}\Big[6(|a_{i-1}|^2 + |b_{i-1}|^2) + \\ 54(|a_i|^2 + |b_i|^2) + 6(|a_{i+1}|^2 + |b_{i+1}|^2) + 13(a_{i-1}\bar{a}_i \\ + b_{i-1}\bar{b}_i + \bar{a}_{i-1}a_i + \bar{b}_{i-1}b_i + a_i\bar{a}_{i+1} + b_i\bar{b}_{i+1} + \bar{a}_i a_{i+1} \\ + \bar{b}_i b_{i+1}) + a_{i-1}\bar{a}_{i+1} + b_{i-1}\bar{b}_{i+1} + \bar{a}_{i-1}a_{i+1} + \bar{b}_{i-1}b_{i+1}\Big] \\ L_i - l_i = 0, \quad \forall i = 1, \cdots, N\end{aligned} \tag{8}$$

Here, the segment length constraints provide N equations. Consequently, the total number of slope and length constraint equations is $(4N+3)$. For the remaining five degrees of freedom a global energy function is defined as

$$f(a,b) = \sum_{i=1}^{n} \left(|a_{i-1} - 2a_i + a_{i+1}|^2 + |b_{i-1} - 2b_i + b_{i+1}|^2\right) \tag{9}$$

The shape estimation problem is formulated as a constrained optimization problem that minimizes the energy function for the $(4N+8)$ unknowns (a, b)

$$\begin{aligned}&\min_{a,b} f(a,b) \\ &\text{s.t.} \quad \boldsymbol{g}_i - \boldsymbol{d}_i = 0, L_j - l_j = 0\end{aligned} \tag{10}$$

This is a nonlinear optimization problem that will be solved using numerical solvers like MATLAB®.

C. Initialization for Numerical Optimization

The numerical optimization of (10) requires initialization of the $(4N+8)$ unknowns. Methodical initialization is critical as unknowns are related through the nonlinear constraints. The three-fold approach involves

1) *Approximating the constraints in terms of unknowns*. The relationship between consecutive a_i, b_i is assumed to be

$$\begin{aligned}a_{i-1} = a_i - \delta a_i, \quad b_{i-1} = b_i - \delta b_i \\ a_{i+1} = a_i + \delta a_{i+1}, \quad b_{i+1} = b_i + \delta b_{i+1}\end{aligned} \tag{11}$$

Substituting (11) in (7), (8) and ignoring the higher order terms corresponding to $\delta a_i, \delta b_i$, the constraint equations can be approximated as

$$\begin{bmatrix} |a_i|^2 - |b_i|^2 \\ 2Re(a_i\bar{b}_i) \\ 2Im(a_i\bar{b}_i) \end{bmatrix} = \boldsymbol{d}_i, \quad |a_i|^2 + |b_i|^2 = l_i \tag{12}$$

2) *Solving approximate constraint equations.* A set of solutions satisfying (12) is

$$\begin{aligned}|a_i|^2 = \frac{1}{2}\psi_i(|\boldsymbol{d}_i| + dx_i), \ |b_i|^2 = \frac{1}{2}\psi_i(|\boldsymbol{d}_i| - dx_i) \\ a_i\bar{b}_i = \frac{1}{2}\psi_i(dy_i + idz_i), \ \text{s.t. } \psi_i = \frac{l_i}{|\boldsymbol{d}_i|}\end{aligned} \tag{13}$$

where a_i, b_i are

$$\begin{aligned}a_i = \sqrt{\frac{1}{2}\psi_i(|\boldsymbol{d}_i| + dx_i)}\exp^{i(\theta_i+\phi_i)} \\ b_i = \sqrt{\frac{1}{2}\psi_i(|\boldsymbol{d}_i| - dx_i)}\exp^{i(\phi_i)} \\ \text{where } \theta_i = \arctan\left(\frac{dz_i}{dy_i}\right) \\ \sin\theta_i = \frac{dz_i}{\sqrt{dy_i^2 + dz_i^2}}, \cos\theta_i = \frac{dy_i}{\sqrt{dy_i^2 + dz_i^2}}\end{aligned} \tag{14}$$

and ϕ_i is a free parameter.

3) *Calculating the free parameters.* We assume $\phi_1 = 0$ and the remaining are obtained by minimizing $\left(|\Delta a_i|^2 + |\Delta b_i|^2\right)$ to minimize the errors of approximation assumption. For ease of calculation, $\Delta\phi_i = \phi_i - \phi_{i-1}$ and $\Delta\theta_i = \theta_i - \theta_{i-1}$

$$\begin{aligned}|\Delta a_i|^2 + |\Delta b_i|^2 = \psi_{i-1}|\boldsymbol{d}_{i-1}| + \psi_i|\boldsymbol{d}_i| - \sqrt{\psi_{i-1}\psi_i} \\ \Big(\sqrt{(\boldsymbol{d}_{i-1} - dx_{i-1})(\boldsymbol{d}_i - dx_i)}\cos(\Delta\phi_i) \\ + \sqrt{(\boldsymbol{d}_{i-1} + dx_{i-1})(\boldsymbol{d}_i + dx_i)}\cos(\Delta\theta_i + \Delta\phi_i)\Big)\end{aligned} \tag{15}$$

Analytically, the minima is found equating the derivative of the above expression with respect to $\Delta\phi_i$ with zero.

$$\tan(\Delta\phi_i^*) = \frac{-\sin(\Delta\theta_i)}{\cos(\Delta\theta_i) + \sqrt{\frac{(\boldsymbol{d}_{i-1} - dx_{i-1})(\boldsymbol{d}_i - dx_i)}{(\boldsymbol{d}_{i-1} + dx_{i-1})(\boldsymbol{d}_i + dx_i)}}} \tag{16}$$

Solving for ϕ_i from the above expression will yield two values due to the square root present in the denominator. The value yielding the minimum when substituted into (15) is taken.

D. Algorithmic Summary

We summarize the shape estimation process as:

(Input) The slopes $\boldsymbol{d}_i$ at the $(N+1)$ knots and the lengths l_i of N segments.

Initializing $(4N+8)$ *unknowns*

(Step 1) Find θ_i using $\sin\theta_i$, $\cos\theta_i$ from (14)

(Step 2) Find the ϕ_i by assuming $\phi_1 = 0$ and calculating $\Delta\phi_i$ using (16)

(Step 3) Initialize a_i and b_i where $i = 1, ..., n$. At this point, a_0, a_{n+1}, b_0 and b_{n+1} are not initialized. These are initialized as

$$\begin{aligned} a_0 &= 2a_1 - a_2, \quad b_0 = 2b_1 - b_2 \\ a_{n+1} &= 2a_n - a_{n-1}, \quad b_{n+1} = 2b_n - b_{n-1} \end{aligned} \tag{17}$$

Optimize the constrained energy function

(Step 4) The nonlinear constrained energy cost function, (10), is minimized using off the shelf solvers like MATLAB®.

(Step 5) α_i and β_i polynomial functions are obtained using (6).

(Step 6) The polynomials for each curve segment are instantaneously obtained using

$$\boldsymbol{r}_i(h) = \int_0^1 \begin{bmatrix} |\alpha_i(h)|^2 - |\beta_i(h)|^2 \\ 2\mathit{Re}\left(\alpha_i(h)\bar{\beta}_i(h)\right) \\ 2\mathit{Im}\left(\alpha_i(h)\bar{\beta}_i(h)\right) \end{bmatrix} dh \tag{18}$$

where $\boldsymbol{r}_i(1) = \boldsymbol{r}_{i+1}(0),\ \forall\ i \in [1, N-1]$ to ensure C^0 continuity.

III. Simulation and Experiments

We analyze the proposed algorithm for two planar scenarios (1) simulated curve with five segments and six knots, and (2) experimental tensegrity spine-like soft manipulator in static orientation with three segments and four knots that are visually observed through a camera. Thereafter, we investigate the robustness of the algorithm to error in the slope angles.

A. Simulation

Simulation is performed in MATLAB®where the algorithm uses `fmincon` function to perform the constrained shape optimization. The computer has Intel®i7 2.90 GHz processor with 8 cores CPU. However, only one core was used in the entire study. A usual optimization process takes utmost 0.029 seconds. All the constraints and cost function are programmed while the derivatives or normalized derivatives (direction cosines), length of each segment for all segments are required as input as discussed in Sec. II-D.

To simulate the accuracy of the algorithm, a quintic 2D curve ('ground truth') is created in Autodesk®Fusion 360 and the slopes are extracted at the knots. Direction cosines are then calculated from slopes $\tan\gamma_i$.

$$\boldsymbol{d}_i = \left[\cos\gamma_i, \sin\gamma_i, 0\right]^T$$

The total length of the curve is $23\ in$ with five equal segments of $4.6\ in$. For true values of the slope, the algorithm is able to successfully reconstruct the true curve, Fig. 2. All the sensors exhibit different accuracy with noise. Consequently, we examine the robustness of the shape estimate by introducing variations in the slope angle, $\delta\gamma_i$

$$\widehat{\boldsymbol{d}_i} = \begin{bmatrix} \cos\left(\gamma_i + \delta\gamma_i\right) \\ \sin\left(\gamma_i + \delta\gamma_i\right) \\ 0 \end{bmatrix}, \quad \delta\gamma_i = \frac{\text{variation}}{100}\gamma_i \tag{19}$$

The slope angle is varied between -5% and 5% of the angle, and the curve is reconstructed, Fig. 2. The error in the position of the ith knot, e_i, is defined as the norm of the difference between the true and the estimated position. The simulation results show increase in e_i with the distance from the base of the manipulator. This can be explained by propagation of the angular error over the manipulator length. We also observe the error normalized to the distance of the knot from the base (first knot), i.e., $\epsilon_i = \dfrac{e_i}{\sum l_i}$. The stability of this normalized position error, Fig. 2c, highlights the robustness of the algorithm. During the simulation, it was observed that strategic initializing of the complex coefficients as discussed may not always yield faster results.

B. Experiments

We used a tensegrity-spine as a soft manipulator to validate the shape estimation algorithm. Tensegrity systems combine tension with compression elements to attain structural integrity [23]. In our case, we construct the tensegrity-spine using wood (compression element) and elastic nylon cables (tension element). The tower uses two $2.5\ in$ outer diameter semicircles with an internal diameter of $1.25\ in$ that will be called sub-vertebrae. These sub-vertebrae have four holes that are used to attach the cables to the rigid wood element. The high deformability and shape change of the tensegrity-spine is achieved by adjusting the control cables connected to each vertebra. The tensegrity-spine has six degrees of freedom where the shape is controlled using these four tendons located along the outer diameter of the tower, Fig. 3. The manipulator can be maneuvered into different shapes by controlling the length of the cord on the vertebrae. In this paper, two planar poses in static configuration are investigated. Each pose is tracked using visual markers located at the knots. Hence, each pose is constructed using three segments. Direction cosines are extracted visually and the length between the markers i.e., knots are calculated. These parameters are then fed to the simulation to generate the shape. The segment length and visually obtained direction cosines of the two poses are tabulated in Tab. I.

The change in the total spine length between the two poses is attributed to the slippage of the central cable of the prototype during reorientation.

C. Result/Discussion

We compare the two poses by observing the Euclidean distance between the estimated and true visually observed knots. The distance error is tabulated in Tab. II.

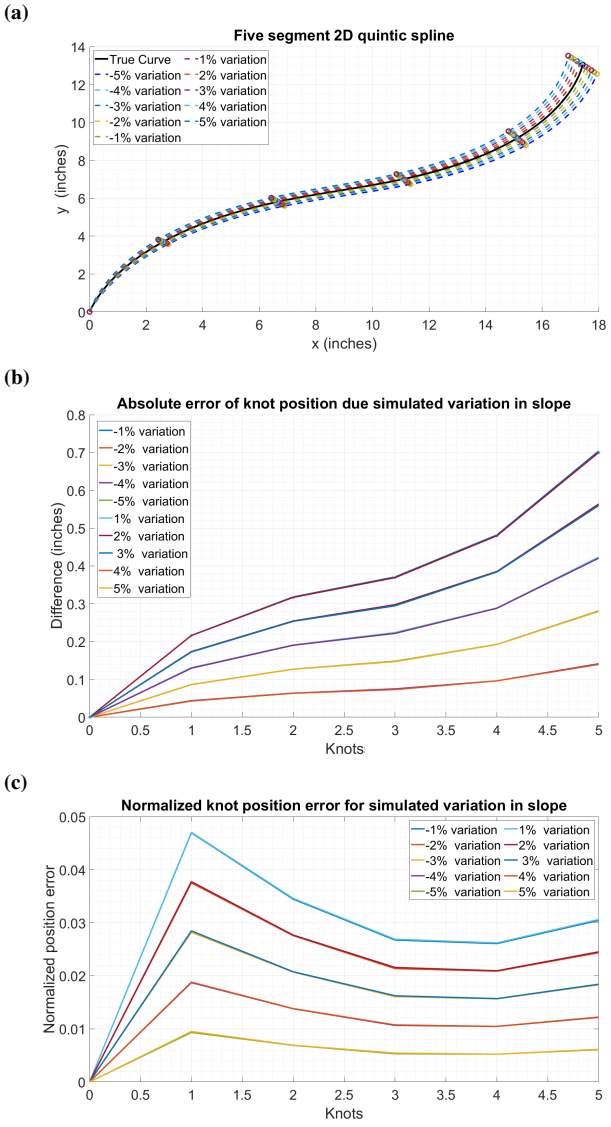

Fig. 2. The simulation of the five segment planar quintic splines estimated using the proposed shape estimation algorithm. (a) The estimated curve shapes as the direction cosines are varied between 95% and 105% of the simulated value. (b) The error between the simulated and the estimated position of the knot. (c) The estimation error normalized to the position of the knot along the manipulator.

The experimental results show the RMS(Root Mean Square) error of $0.863in$ and $0.851in$ for the two tensegrity manipulator poses. The Fig. 3 illustrates the estimated manipulator shape and the position of the knots. The estimation error at the end-effector (knot 4) position is observed to be maximum. The relative position errors (normalized with the manipulator length) are 6.53% and 6.2% for the two poses. The error in visual measurement of the slope is analyzed by varying all the slopes by 5% of the respective angles (as done for simulations). This also illustrates the robustness of the nonlinear optimization approach to errors and variation of the slope.

TABLE I
EXPERIMENTAL POSES DATA

Pose 1			
Segment	**Length** (in)	**Knot**	**Direction cosine**
l_1	5.93	1	$[0.0217, 0.9998, 0]^T$
l_2	5.59	2	$[0.8421, 0.5393, 0]^T$
l_3	5.86	3	$[0.6711, 0.7414, 0]^T$
		4	$[0.0446, 0.999, 0]^T$
Pose 2			
Segment	**Length** (in)	**Knot**	**Direction cosine**
l_1	6.19	1	$[0.0809, 0.9967, 0]^T$
l_2	5.76	2	$[0.9094, 0.4159, 0]^T$
l_3	6.09	3	$[0.9853, 0.1707, 0]^T$
		4	$[0.8908, 0.4544, 0]^T$

TABLE II
EXPERIMENTAL ERROR BETWEEN ESTIMATED AND TRUE KNOTS (in)

Knot	1	2	3	4	**RMS**
Pose 1	0	0.906	0.356	1.135	0.863
Pose 2	0	0.663	0.693	1.119	0.851

IV. CONCLUSION

The paper discusses shape estimation of a soft manipulator modeled using piecewise continuous curvature PH curves. This is formulated as a constrained nonlinear optimization constrained with slope and length constraints. We simulate and experimentally validate the multi-segment modeling of soft manipulators on a tensegrity-spine manipulator. The simulation involves use of six segments while the experiments use three segments with visual markers on the manipulator. The algorithm illustrates robustness to simulated variations in the slopes and end-effector relative distance error of 6.53% and 6.2% for the two poses.

Future work will involve investigation of the PH-curve model to estimate the 3-dimensional shape and the use of IMUs for obtaining slopes.

REFERENCES

[1] R. J. Webster and B. A. Jones, "Design and Kinematic Modeling of Constant Curvature Continuum Robots: A Review," *The International Journal of Robotics Research*, vol. 29, pp. 1661–1683, Nov. 2010.

[2] I. Walker, "Continuum robot appendages for traversal of uneven terrain in in situ exploration," in *IEEE Aerospace Conference*, pp. 1–8, Mar. 2011.

[3] G. Krishnan, J. Bishop-Moser, C. Kim, and S. Kota, "Kinematics of a Generalized Class of Pneumatic Artificial Muscles," *Journal of Mechanisms and Robotics*, vol. 7, pp. 041014–041014–9, Nov. 2015.

[4] N. Simaan, "Snake-Like Units Using Flexible Backbones and Actuation Redundancy for Enhanced Miniaturization," in *Proceedings of the 2005 IEEE International Conference on Robotics and Automation*, pp. 3012–3017, Apr. 2005.

[5] N. K. Uppalapati, B. Walt, A. Havens, A. Mahdian, G. Chowdhary, and G. Krishnan, "A berry picking robot with a hybrid soft-rigid arm: Design and task space control," in *Robotics: Science and System*, 2020.

[6] B. A. Jones and I. D. Walker, "Kinematics for multisection continuum robots," *IEEE Transactions on Robotics*, vol. 22, pp. 43–55, Feb. 2006. Conference Name: IEEE Transactions on Robotics.

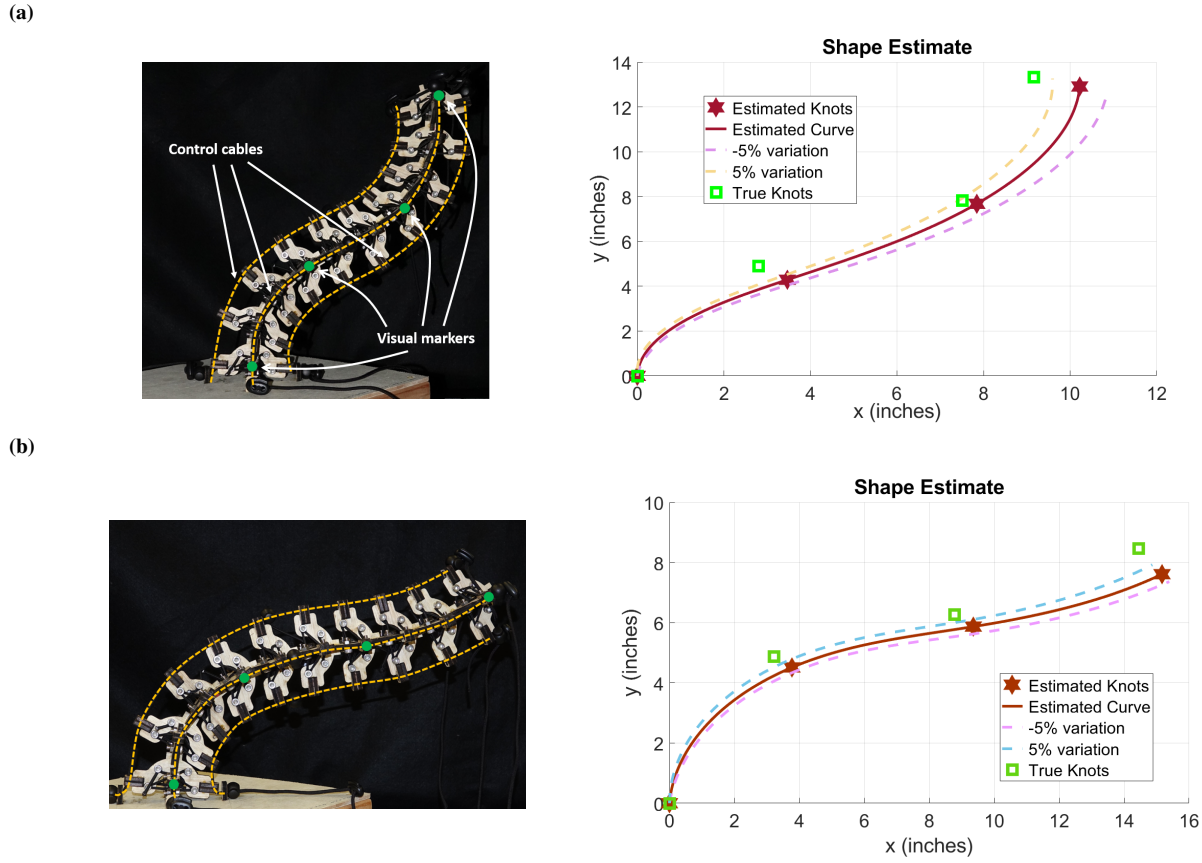

Fig. 3. The tensegrity-spine manipulator with visual markers (in green) that indicate the knots. The control cables are highlighted by orange dotted line and manipulate the manipulator shape. (a-b) The two experimental poses estimated using the proposed algorithm and the robustness of the algorithm to the variations in the slope (sensor noise).

[7] F. Renda, C. Armanini, V. Lebastard, F. Candelier, and F. Boyer, "A Geometric Variable-Strain Approach for Static Modeling of Soft Manipulators With Tendon and Fluidic Actuation," *IEEE Robotics and Automation Letters*, vol. 5, pp. 4006–4013, July 2020. Conference Name: IEEE Robotics and Automation Letters.

[8] D. Zappetti, R. Arandes, E. Ajanic, and D. Floreano, "Variable-stiffness tensegrity spine," *Smart Materials and Structures*, vol. 29, p. 075013, June 2020. Publisher: IOP Publishing.

[9] A. P. Sabelhaus, A. K. Akella, Z. A. Ahmad, and V. SunSpiral, "Model-Predictive Control of a flexible spine robot," in *2017 American Control Conference (ACC)*, pp. 5051–5057, May 2017.

[10] T. Giffney, M. Xie, A. Yong, A. Wong, P. Mousset, A. McDaid, and K. Aw, "Soft Pneumatic Bending Actuator with Integrated Carbon Nanotube Displacement Sensor," *Robotics*, vol. 5, p. 7, Mar. 2016. Number: 1 Publisher: Multidisciplinary Digital Publishing Institute.

[11] K. Elgeneidy, N. Lohse, and M. Jackson, "Bending angle prediction and control of soft pneumatic actuators with embedded flex sensors – A data-driven approach," *Mechatronics*, vol. 50, pp. 234–247, Apr. 2018.

[12] J. So, U. Kim, Y. B. Kim, D.-Y. Seok, S. Y. Yang, K. Kim, J. H. Park, S. T. Hwang, Y. J. Gong, and H. R. Choi, "Shape Estimation of Soft Manipulator Using Stretchable Sensor," *Cyborg and Bionic Systems*, vol. 2021, Apr. 2021. Publisher: Science Partner Journal.

[13] R. J. Roesthuis and S. Misra, "Steering of Multisegment Continuum Manipulators Using Rigid-Link Modeling and FBG-Based Shape Sensing," *IEEE Transactions on Robotics*, vol. 32, pp. 372–382, Apr. 2016. Conference Name: IEEE Transactions on Robotics.

[14] H. Wang, R. Zhang, W. Chen, X. Liang, and R. Pfeifer, "Shape Detection Algorithm for Soft Manipulator Based on Fiber Bragg Gratings," *IEEE/ASME Transactions on Mechatronics*, vol. 21, pp. 2977–2982, Dec. 2016. Conference Name: IEEE/ASME Transactions on Mechatronics.

[15] H. Zhao, K. O'Brien, S. Li, and R. F. Shepherd, "Optoelectronically innervated soft prosthetic hand via stretchable optical waveguides," *Science robotics*, vol. 1, no. 1, p. eaai7529, 2016. Publisher: Science Robotics.

[16] W. Zhuang, G. Sun, H. Li, X. Lou, M. Dong, and L. Zhu, "FBG based shape sensing of a silicone octopus tentacle model for soft robotics," *Optik*, vol. 165, pp. 7–15, July 2018.

[17] Q. Hou, C. Lu, and X. Li, "A novel pose sensing model for soft manipulator based on helical FBG," *Sensors and Actuators A: Physical*, vol. 321, p. 112586, Apr. 2021.

[18] A. AlBeladi, G. Krishnan, M.-A. Belabbas, and S. Hutchinson, "Vision-Based Shape Reconstruction of Soft Continuum Arms Using a Geometric Strain Parametrization," *arXiv:2011.09106 [cs]*, Nov. 2020. arXiv: 2011.09106.

[19] S. Nathalie, D. Dominique, L. Bernard, and B. Luc, "Curve Reconstruction via a Ribbon of Sensors," in *2007 14th IEEE International Conference on Electronics, Circuits and Systems*, pp. 407–410, Dec. 2007.

[20] R. T. Farouki, *Pythagorean-Hodograph Curves: Algebra and Geometry Inseparable*. Geometry and Computing, Berlin Heidelberg: Springer-Verlag, 2008.

[21] M. Huard, R. T. Farouki, N. Sprynski, and L. Biard, "C2 interpolation of spatial data subject to arc-length constraints using Pythagorean–hodograph quintic splines," *Graphical Models*, vol. 76, pp. 30–42, Jan. 2014.

[22] I. Singh, Y. Amara, A. Melingui, P. Mani Pathak, and R. Merzouki, "Modeling of Continuum Manipulators Using Pythagorean Hodograph Curves," *Soft Robotics*, vol. 5, pp. 425–442, Aug. 2018. Publisher: Mary Ann Liebert, Inc., publishers.

[23] R. Motro, *Tensegrity: structural systems for the future*. Elsevier, 2003.